REVIEWS

Journal of Semiconductors
(2020) 41, 051201
doi: 10.1088/1674-4926/41/5/051201

Recent progress in developing efficient monolithic all-perovskite tandem solar cells

Yurui Wang‡, Mei Zhang‡, Ke Xiao, Renxing Lin, Xin Luo, Qiaolei Han, and Hairen Tan†

National Laboratory of Solid State Microstructures, Jiangsu Key Laboratory of Artificial Functional Materials, College of Engineering and Applied Sciences, Nanjing University, Nanjing 210093, China

Abstract: Organic–inorganic halide perovskites have received widespread attention thanks to their strong light absorption, long carrier diffusion lengths, tunable bandgaps, and low temperature processing. Single-junction perovskite solar cells (PSCs) have achieved a boost of the power conversion efficiency (PCE) from 3.8% to 25.2% in just a decade. With the continuous growth of PCE in single-junction PSCs, exploiting of monolithic all-perovskite tandem solar cells is now an important strategy to go beyond the efficiency available in single-junction PSCs. In this review, we first introduce the structure and operation mechanism of monolithic all-perovskite tandem solar cell. We then summarize recent progress in monolithic all-perovskite tandem solar cells from the perspectives of different structural units in the device: tunnel recombination junction, wide-bandgap top subcell, and narrow-bandgap bottom subcell. Finally, we provide our insights into the challenges and scientific issues remaining in this rapidly developing research field.

Key words: perovskite solar cells; monolithic tandem; monolithic all-perovskite tandem solar cell; stability

Citation: Y R Wang, M Zhang, K Xiao, R X Lin, X Luo, Q L Han, and H R Tan, Recent progress in developing efficient monolithic all-perovskite tandem solar cells[J]. *J. Semicond.*, 2020, 41(5), 051201. http://doi.org/10.1088/1674-4926/41/5/051201

1. Introduction

Organic–inorganic metal halide perovskites have become attractive light absorber materials for solar cells due to their high optical absorption coefficient, long carrier diffusion length, low trap density, tunable bandgap, and simple processing[1–8]. The power conversion efficiency (PCE) of single-junction perovskite solar cells (PSCs) has increased from 3.8% to 25.2% in just a decade[9–11].

Fabricating tandem solar cells by combining subcells with different bandgaps offers an avenue to go beyond the Shockley-Queisser limit[12] of single-junction solar cells. The highest PCE of 47.1% among all photovoltaic cells has been achieved by a multi-junction solar cell with six subcells made of III–V compound semiconductors[10, 11, 13]. Nonetheless, these devices are not commercially viable for terrestrial applications because of their complex manufacturing and extremely high costs[14, 15]. Organic tandem solar cells offer potential of much lower fabrication costs because of their simple solution processability. However, the PCEs of organic photovoltaics are far below those available in inorganic devices[16–19]. Metal halide perovskites have become ideal candidates for fabricating tandem solar cells because they have demonstrated both high PCEs and low costs in single-junction PSCs.

The bandgap tunability enables metal halide perovskites to construct perovskite-perovskite (all-perovskite) tandem solar cells[20]. A wide-bandgap perovskite is used for the top subcell while a narrow-bandgap perovskite is used for the bottom subcell. The bandgap of Pb halide perovskite can be continuously tuned from 1.5 to 2.5 eV by adjusting the I/Br ratio[21–24], making them suitable for top subcells in tandem solar cells. Meanwhile, the bandgap of mixed Pb–Sn perovskites can be lowered to ~1.2 eV by adjusting the composition of the B-site metal cation[25–31]. In addition to the application on all-perovskite tandem solar cells, wide-bandgap perovskites have been deployed in perovskite/silicon[32–36], perovskite/Cu (In, Ga) Se_2 (CIGS)[37–42], and other tandem configurations[43–45]. Overall, all-perovskite tandem solar cells have the potential of offering lower fabrication cost, less environmental impact, and higher PCE than other perovskite-based tandem structures[46–51].

In the early stage, all-perovskite tandem solar cells showed much lower performance compared to single-junction PSCs[52]. With improvement in the growth of mixed Pb–Sn narrow-bandgap perovskites, Snaith *et al.* firstly demonstrated a PCE of 16.9% by monolithically combining a narrow-bandgap perovskite ($FA_{0.75}Cs_{0.25}Sn_{0.5}Pb_{0.5}I_3$) with a wide-bandgap perovskite[53]. Very recently, our group has developed a strategy to improve the performance and stability of all-perovskite tandem solar cells via a comproportionation reaction for the growth of mixed Pb–Sn perovskites. This enabled us to achieve high PCEs of 24.8% and 22.1% for small-area (0.073 cm^2) and large-area (1.048 cm^2) tandem solar cells, respectively[54]. The PCE evolution of all-perovskite tandem solar cells in the past five years is presented in Fig. 1. The PCE of all-perovskite tandem solar cells is now approaching that of best-performing single-junction PSCs (24.8%[54] versus 25.2%[10]).

Here we give a short review on recent research progress in improving the efficiency of all-perovskite tandem solar cells. In Section 2, we present the structure and working mechanism of all-perovskite tandem solar cell. Fig. 1 and Table 1 show the PCE evolution of all-perovskite tandem sol-

Yurui Wang and Mei Zhang contributed equally to this work.
Correspondence to: H R Tan, hairentan@nju.edu.cn
Received 1 MARCH 2020; Revised 17 MARCH 2020.

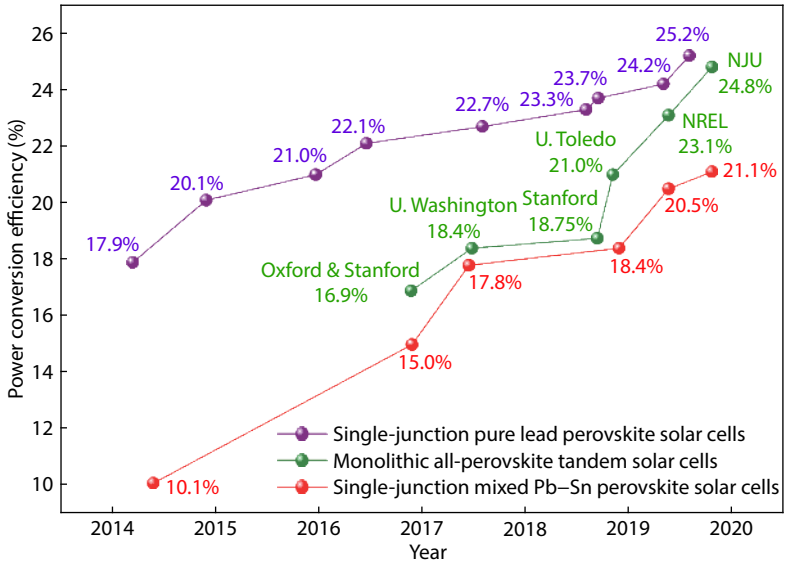

Fig. 1. (Color online) The PCE evolution of single-junction PSCs and all-perovskite tandem solar cells.

Table 1. Structure, bandgap matching, and performance parameters of all-perovskite tandem solar cells.

Year	Device structure	Bandgap matching (eV/eV)	PCE (%)	V_{oc} (V)	J_{sc} (mA/cm^2)	FF (%)	Area (cm^2)	Ref.
2015	FTO/bl-TiO_2/$MAPbBr_3$/HTM/PEDOT:PSS/$MAPbI_3$/PCBM/Au	2.25/1.55	10.4	2.25	8.3	56	0.0960	[52]
2016	ITO/NiO_x/$FA_{0.83}Cs_{0.17}PbI_{0.83}Br_{0.17}$/PCBM/$SnO_2$/ZTO/ITO/PEDOT:PSS/$FA_{0.75}Cs_{0.25}Sn_{0.5}Pb_{0.5}I_3$/PCBM/BCP/Ag	1.80/1.20	16.9	1.66	14.5	70	0.2000	[53]
2017	ITO/NiO_x/$MA_{0.9}Cs_{0.1}Pb(I_{0.6}Br_{0.4})_3$/$C_{60}$/Bis-$C_{60}$/ITO/ PEDOT:PSS/$MASn_{0.5}Pb_{0.5}I_3$/$IC_{60}BA$/Bis-$C_{60}$/Ag	1.80/1.20	18.4	1.98	12.7	73	0.1000	[73]
2018	ITO/PTAA/$FA_{0.6}Cs_{0.4}Pb(I_{0.7}Br_{0.3})_3$/$C_{60}$/$SnO_2$/ITO/PEDOT:PSS/$FA_{0.75}Cs_{0.25}Sn_{0.5}Pb_{0.5}I_3$/$C_{60}$/BCP/Ag	1.76/1.27	18.7	1.81	14.8	70	/	[75]
2018	ITO/PTAA/$FA_{0.8}Cs_{0.2}Pb(I_{0.7}Br_{0.3})_3$/$C_{60}$/BCP/Ag/$MoO_x$/ITO/PEDOT:PSS/$(FASnI_3)_{0.6}(MAPbI_3)_{0.4}$/PCBM/BCP/Ag	1.75/1.25	21.0	1.92	14	78	0.1050	[76]
2019	ITO/PTAA/$(FA_{0.8}Cs_{0.2}Pb(I_{0.7}Br_{0.3})_3$/$C_{60}$/BCP/Ag/$MoO_x$/ITO/PEDOT:PSS/$(FASnI_3)_{0.6}(MAPbI_3)_{0.4}$/PCBM/BCP/Ag	1.75/1.25	23.4	1.94	15.0	80	0.1050	[77]
2019	ITO/PolyTPD/PFN-Br/$DMA_{0.1}FA_{0.6}Cs_{0.3}PbI_{2.4}Br_{0.6}$/LiF/$C_{60}$/PEIE/AZO/IZO/PEDOT:PSS/$FA_{0.75}Cs_{0.25}Sn_{0.5}Pb_{0.5}I_3$/$C_{60}$/BCP/Au	1.7/1.27	20.6	1.82	15.33	74	/	[78]
2019	ITO/PTAA/$FA_{0.8}Cs_{0.2}Pb(I_{0.6}Br_{0.4})_3$/$C_{60}$/$SnO_2$/Au/PEDOT:PSS/$FA_{0.7}MA_{0.3}Pb_{0.5}Sn_{0.5}I_3$/$C_{60}$/BCP/Cu	1.77/1.22	24.8	1.96	15.6	81	0.0730	[54]

ar cells in the past few years. In Section 3, we summarize recent progress in improving the efficiency of all-perovskite tandem solar cells in three aspects: tunnel recombination junction, wide-bandgap top subcell, and narrow-bandgap bottom subcell. Finally, we summarize in Section 4 the remaining issues that constrain the performance of all-perovskite tandem solar cells. We thereby provide an outlook and perspective for future development of all-perovskite tandem solar cells.

2. Device structure and working mechanism

2.1. Device structure and working mechanism of all-perovskite tandem solar cell

Unless otherwise stated, tandem solar cells are referred to monolithic two-terminal devices in this review article. The monolithic all-perovskite tandem solar cell includes two subcells: the top subcell made of a wide-bandgap perovskite and the bottom subcell using a narrow-bandgap perovskite, as shown in Fig. 2(a). The subcells are connected with a tunnel recombination junction (also called interconnecting layer or charge recombination junction). The current in subcells should be matched to deliver optimal performance. The photocurrent of tandem solar cells follows the Kirchhoff's law[55], depending on the minimum current in two subcells.

Sunlight consists of a broad energy spectrum with varying intensity, ranging from ultraviolet (photon energy higher than 3 eV) to infrared (photon energy lower than 1.7 eV to about 0.5 eV). When light is incident on a semiconductor, light with energy higher than the bandgap is absorbed, and light with energy lower than the bandgap is passed through without absorption, as shown in Fig. 2(b). The excess energy of the photon (above the bandgap energy) is lost as heat due to electron thermalization. The trade-off between harvesting more photons and minimizing thermalization loss in single-junction photovoltaic devices limits their theoretical maximum PCE (Shockley-Queisser limit)[12, 56].

The working principle of tandem solar cells is to combine two subcells with different bandgaps, thereby absorbing a region of sunlight in each subcell to improve performance by reducing thermalization loss[56]. The schematic of the different spectral distribution is shown in Fig. 2(c). In the tandem solar cell, photons with higher energy are absorbed in

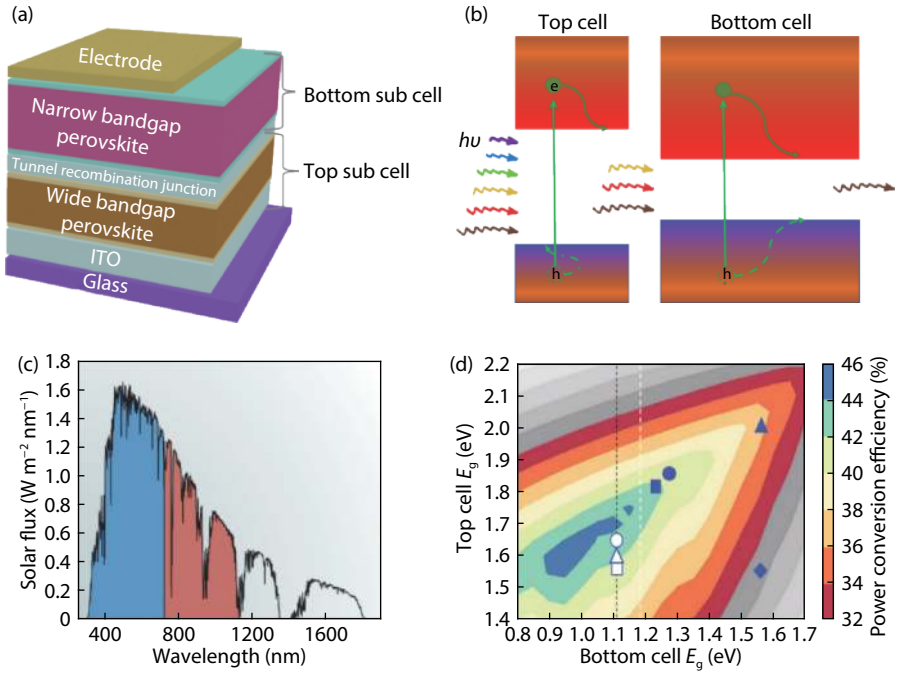

Fig. 2. (Color online) (a) Schematic structure of monolithic all-perovskite tandem solar cells. (b) Absorption of different wavelengths of light by different bandgap subcells. (c) Solar irradiance spectrum showing the spectral regions over which the two semiconductors could absorb. Reproduced with permission[56]. (d) Theoretical efficiency limit for monolithic all-perovskite tandem solar cells, calculated with different subcell thicknesses, each picked to optimize the performance for each bandgap combination. Reproduced with permission[23].

the top subcell, whereas the remaining lower energy photons enter the device and are absorbed by the bottom subcells. Consequently, the combination of perovskites layers with different bandgaps enables maximum utilization of the solar spectrum. Consequently, the theoretical PCE limits are increased to 44.3% for double-junction cells and even higher than 50% for triple-junction cells[57].

Theoretically, the open-circuit voltage (V_{oc}) in a tandem solar cell is nearly the sum of the V_{oc} of two subcells, where the V_{oc} loss is mainly caused by the tunnel recombination junction. The short-circuit current density (J_{sc}) value in the device is the smaller one of two subcells. Furthermore, the thickness of subcells has a significant effect on light capturing and thus the resulting J_{sc}. Both bandgap and absorber thickness matching are required in all-perovskite tandem solar cells to achieve optimal performance. Fig. 2(d) shows the maximum PCE of tandem solar cells with different bandgap matching. For all-perovskite tandem solar cells, the best bandgap matching is considered to be that the bottom subcell has a bandgap around 1.2 eV and the top subcell has a bandgap around 1.8 eV[58]. Performance and bandgap matching in all-perovskite tandem solar cells are summarized in Table 1.

2.2. Bandgap tuning of perovskite materials

Perovskite materials have a general structural formula: ABX_3, A^+ is usually an organic cation, B^{2+} is a metal ion, and X^- is a halogen ion. We list the different substitution types in Fig. 3(a). The bandgap can be continuously tune between 1.2 and 2.5 eV by adjusting the composition[21–24, 27–31, 59].

2.2.1. Pure lead wide-bandgap perovskite

This is the most common strategy to obtain a perovskite material with a wider bandgap by partial substitution of I^- with Br^-. For a typical $MAPbX_3$ perovskite, the bandgap can be continuously widened from 1.58 eV (0%-Br) to 2.28 eV (100%-Br) by increasing the proportion of Br^- at X-site. It can be seen from Fig. 3(b) that when the bromine content in $MAPb(I_{1-x}Br_x)_3$ is gradually increased, the onset absorption band is tuned from 786 to 544 nm[60]. The same tendency is observed in FA-based (Fig. 3(c))[24] and Cs-based (Fig. 3(d))[21] lead halide perovskites. The difference is that $FAPbI_3$ (1.48 eV) has a slightly lower bandgap than $MAPbI_3$ (1.57 eV), while $CsPbI_3$ (1.73 eV) has a slightly wider bandgap than $MAPbI_3$. At the same time, the all-inorganic wide-bandgap perovskite shows the potential of processing stable tandem solar cells[61, 62].

Partial substitution of the A-site using DMA^+ (DMA is dimethylammonium) also leads to widening of the bandgap (Fig. 3(e))[63]. It has been reported that halide segregation in a wide-bandgap perovskite can be effectively suppressed by adjusting the ratio of DMA^+ at the A-site, thereby improving stability of PSCs. Recent studies have shown that alloying $Rb^+/Cs^+/MA^+/FA^+$ at A-site are helpful to improve the photostability under illumination[64–67].

2.2.2. Mixed Pb–Sn narrow-bandgap perovskite

Partial substitution of Sn^{2+} with Pb^{2+} at B-site can further lower the bandgap of tin halide perovskites[25–31]. Freeman *et al.* observed that the $MASn_xPb_{1-x}I_3$ perovskites have a minimum bandgap of 1.17 eV (determined by the absorption onset at 1060 nm, the actual optical bandgap is ~1.25 eV)[69]. Snaith *et al.* found the same trend in $FASn_xPb_{1-x}I_3$ perovskites. For compositions with > 50% Sn content, a special type of the Pb–Sn positions allowed the bandgap to shift lower than the end point, causing the bowing trend[53]. The bandgap tuning by varying the tin content in FA and FA/MA perovskites is shown in Figs. 3(f) and 3(g).

Additionally, the radius of the A-site ion can tune the bandgap of the perovskite by affecting the structure of the lattice[70]. The substitution of MA^+ with FA^+ and Cs^+ at A-site

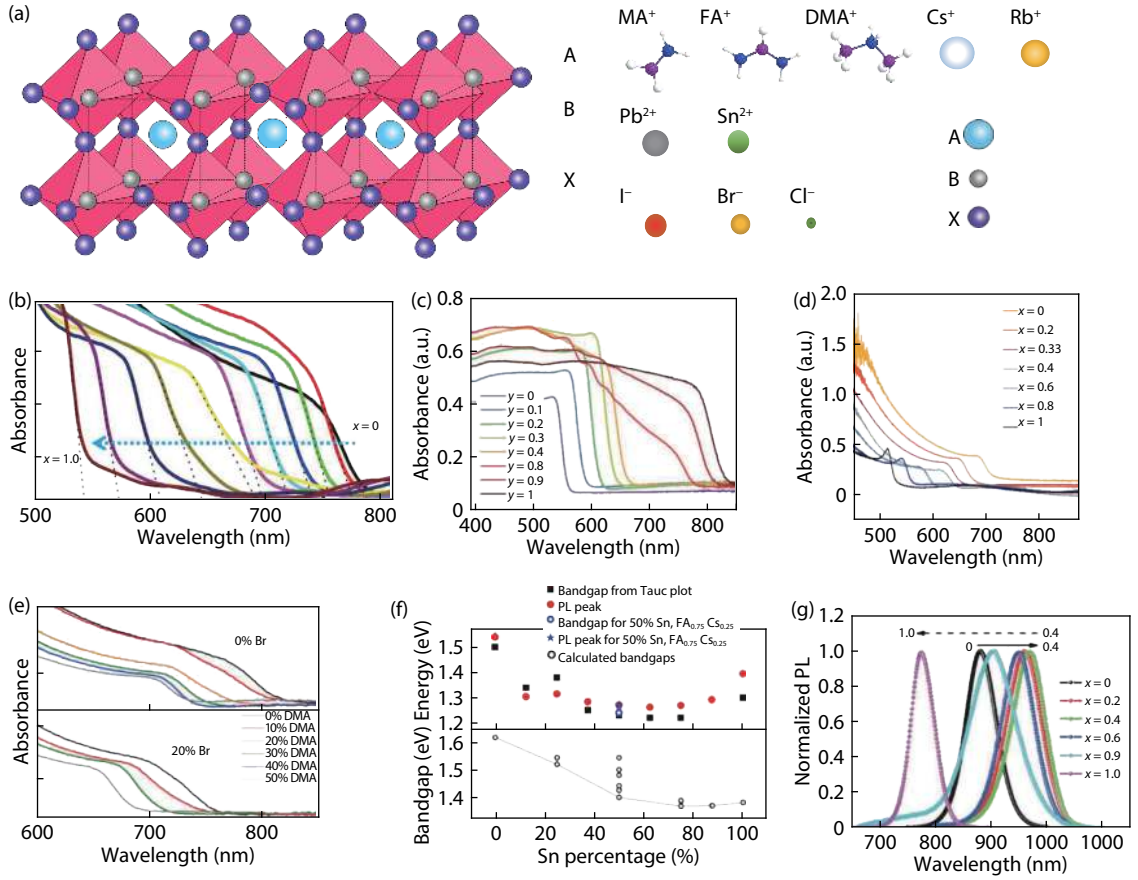

Fig. 3. (Color online) Schematic of the structure and bandgap tuning of perovskite. (a) Perovskite structure and selectable bandgap tuning ions. (b) UV–vis absorption spectra of the $MAPb(I_{1-x}Br_x)_3$. Reproduced with permission[60]. (c) UV–vis absorbance spectra of the $FAPbI_yBr_{3-y}$. Reproduced with permission[24]. (d) Absorption onset in $CsPb(Br_xI_{1-x})_3$ with increasing bromine content. Reproduced with permission[21]. (e) UV–vis absorbance spectra of perovskite films made with increasing DMA percentage of the A-site, with 0% bromine (top) and 20% bromine (below). DMA addition was compensated in an equimolar manner with addition of Cs. Reproduced with permission[63]. (f) Bandgap values obtained from the Tauc plot and PL spectra of $FASn_xPb_{1-x}I_3$ perovskites (top); bandgap values calculated using the first-principles method (bottom). Reproduced with permission[53]. (g) PL spectra of $(FASnI_3)_x(MAPbI_3)_{1-x}$ with different x values. Reproduced with permission[68].

also affects the bandgap. A narrow-bandgap perovskite can be obtained by introducing FA^+ at the A-site, possibly because FA^+ have a slightly larger ionic radius than MA^+[71]. Jen *et al.* achieved improved stability while maintaining high performance for narrow-bandgap Sn-based PSCs by introducing different amounts of FA^+ into $MAPb_{0.75}Sn_{0.25}I_3$[29]. McGehee *et al.* observed an abnormal phenomenon that larger ratio of Cs^+ can slightly reduce the bandgap of $FA_{1-x}Cs_xPb_ySn_{1-y}I_3$ narrow-bandgap perovskites when Sn content is higher than 50%[70].

3. Recent progress in monolithic all-perovskite tandem solar cells

We can divide the structure of all-perovskite tandem solar cells into three crucial parts: the top subcell, the bottom subcell, and the tunnel recombination junction (interconnecting layer). We next summarize the progress in all-perovskite tandem solar cells in these three parts. Details of all-perovskite tandem solar cells developed so far can be found in Table 1.

3.1. Tunnel recombination junction

One challenge in fabricating tandem solar cells is how to protect the top subcells when depositing the bottom subcells using solution processing. A tunnel recombination junction (also known as interconnecting layer) is required for electrical series connection between subcells in all-perovskite tandem solar cells. The tunnel junction must meet following requirements: (1) It must form ohmic contact with the charge extraction layers, promote the recombination of electrons and holes from subcells, and lead to as small series resistance loss as possible. (2) It must be compact enough to protect the top subcell from damage when depositing the bottom subcell. (3) It must have sufficient optical transparence to ensure low parasitic absorption.

The structure of tunnel recombination junction is continuously evolving in the development of all-perovskite tandem solar cells. At present, conductive transparent materials are deployed in tunnel junction for tandem solar cells, such as N4,N4,N4″, N4″-tetra([1,1′-biphenyl]-4-yl)-[1,1′:4′,1″-terphenyl]-4′,4″-diamine(TaTm) doped with 2,2′-(perflfluor-onaphthalene-2,6-diylidene) dimalononitrile(TaTm:F6-TCNNQ), poly(3,4-ethylenedioxythiophene) polystyrene sulfonate (PEDOT:PSS), aluminum doped zinc oxide (AZO), and indium tin oxide (ITO). Deposition techniques include vacuum deposition[72], sputter coating[73] and film transfer lamination[74], thermal evaporation[54] and atomic layer deposition[63].

There are two strategies to avoid damaging the top subcell when the bottom subcell is deposited on top: (1) pro-

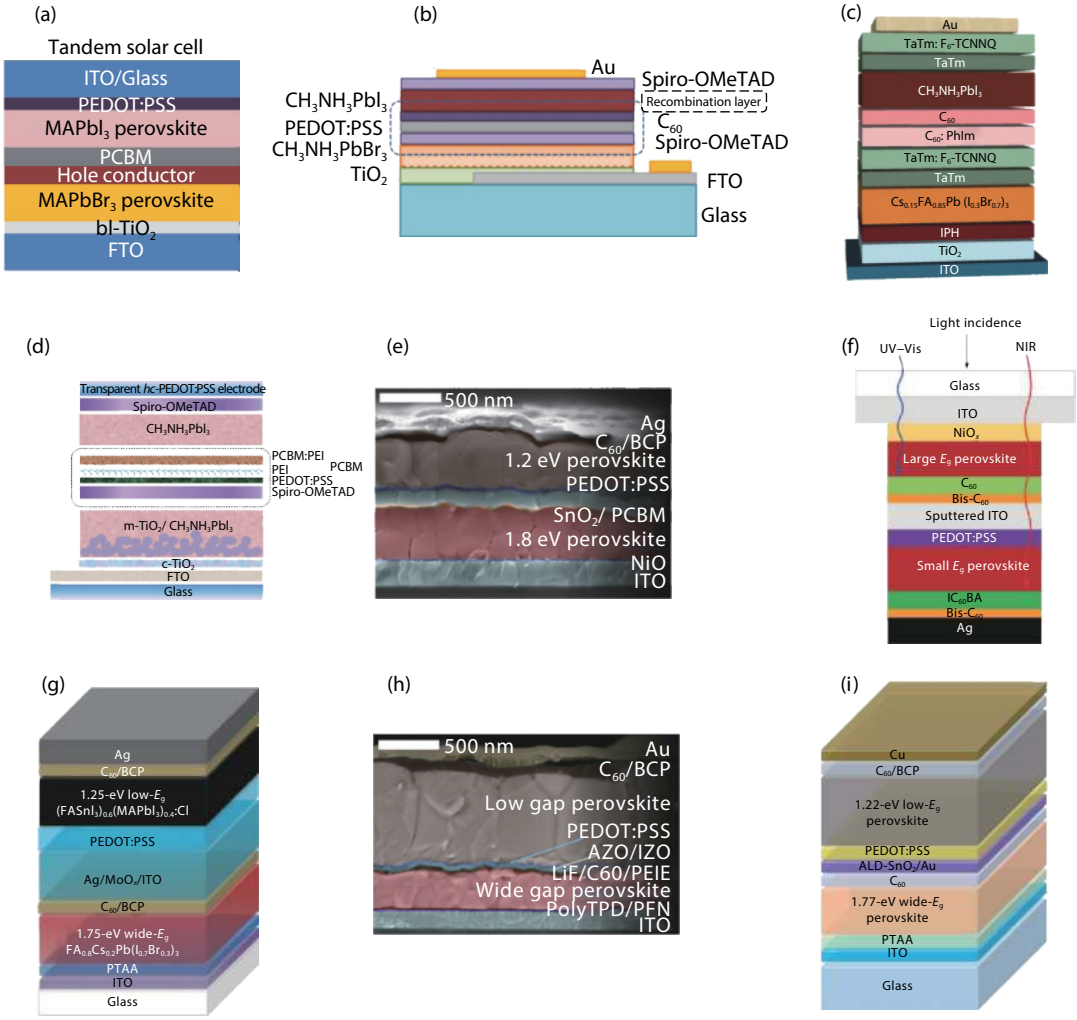

Fig. 4. (Color online) Schematic structures of all-perovskite tandem solar cells with different tunnel recombination junctions. (a) Structure of a tandem solar cell with a lamination for connecting subcells. Reproduced with permission[52]. (b) Structure of a tandem solar cell using PEDOT:PSS as the charge recombination layer. Reproduced with permission[79]. (c) Structure of a tandem solar cell using TaTm:F6-TCNNQ as the charge recombination layer. Reproduced with permission[72]. (d) Structure of a tandem solar cell using spiro-OMeTAD/PEDOT: PSS/PEI/PCBM: PEI as the tunnel recombination junction. Reproduced with permission[74]. (e) Cross-section SEM images of a tandem solar cell using ITO as the charge recombination layer and SnO_2 as the buffer layer. Reproduced with permission[53]. (f) Structure of a tandem solar cell using ITO as the charge recombination layer and Bis-C_{60} as the buffer layer. Reproduced with permission[73]. (g) Structure of a tandem solar cell using ITO as the charge recombination layer and Ag/MoO_3 as the buffer layer. Reproduced with permission[76]. (h) Cross-sectional SEM of a tandem solar cell using AZO/IZO as the charge recombination layer. Reproduced with permission[63]. (i) Structure of a tandem solar cell using Au/SnO_2 as the tunnel recombination junction. Reproduced with permission[54].

cess the bottom subcell using non-solution approach; and (2) deploy a dense tunnel recombination junction to prevent the solvent from damaging the top subcell. We will introduce the recent progress of tunnel recombination junction used in all-perovskite tandem solar cells from following three aspects.

3.1.1. Lamination for connecting subcells

Im *et al.* used a 2-micron hole-transport layer (PEDOT: PSS) as a recombination layer in their early work to assemble two independent subcells by lamination, as shown in Fig. 4(a)[52]. Because of the lack of dense tunnel recombination junction to protect the top subcell, non-orthogonal solvents (specifically, dimethyl formamide (DMF) and dimethyl sulfoxide (DMSO)) cannot be used to deposit the bottom subcell without damaging the top subcell.

3.1.2. Tunnel junction for bottom subcell processed by non-solution methods

Vacuum deposition is a useful way to process perovskite films. Snaith *et al.* used spin-coated PEDOT:PSS as the tunnel recombination junction, as shown in Fig. 4(b). PbI_2 films were deposited by thermal evaporation on top of the front subcell, and then converted to perovskite by reacting with MAI in isopropanol solution through interdiffusion[79]. However, the thickness of the perovskite layer is only about 200 nm due to the limited penetration of MAI.

Other tunnel recombination junctions have also been reported to protect top subcells when processing bottom subcells using vacuum deposition. Sessolo *et al.* developed the N4, N4, N4″, N4″ -tetra([1,1′-biphenyl]-4-yl)-[1,1′: 4′, 1″ -terphenyl] -4,4″ -diamine(TaTm) as the charge recombination layer, whose conductivity can be increased by two orders of magnitude after doping with 2,2′-(Perfluoronaphthalene-2,6-diylidene) dimalononitrile (F6-TCNNQ)[72]. The structure of this device is shown in Fig. 4(c). Vacuum deposition was used to deposit $MAPbI_3$ onto the wider bandgap perovskite sub-

cell with a composition of $Cs_{0.15}FA_{0.85}Pb(I_{0.3}Br_{0.7})_3$. The champion device achieved a PCE of 18% with a relatively low matched J_{sc} value of only 9.2 mA/cm^2. In another work by Bolink *et al*., F6-TCNNQ-doped TaTm was also chose as the charge recombination layer. The thickness of the top and the bottom $CH_3NH_3PbI_3$ layer were relatively different (95 and 420 nm) by controlling the vacuum deposition process[80, 81]. The tandem solar cell achieved a high PCE of 18.02% but a low J_{sc} value of 9.84 mA/cm^2. When vacuum deposition is used to process the bottom cell, a particularly dense tunnel recombination junction is not required because there is no potential solvent to damage the top cell. This advantage makes it a potential strategy to fabricate all-perovskite tandem solar cells. However, efficient mixed Pb–Sn narrow-bandgap PSCs are challenging to process using vacuum deposition approach.

3.1.3. Dense tunnel recombination junction for full solution processing of perovskites

Processing a dense tunnel recombination junction is considered to be the best strategy to protect the top subcell from solvents in subsequent processing. In 2015, Zhou *et al*. firstly demonstrated bottom-up solution-processed all-perovskite tandem solar cells via designing a novel tunnel recombination junction: Spiro-OMeTAD/PEDOT:PSS/PEI/PCBM:PEI, as shown in Fig. 4(d). This tunnel recombination junction is efficient to collect electrons and holes from its top and bottom subcells, and robust enough to protect the top perovskite film during the bottom perovskite film deposition[74]. The use of sputtered ITO offers another candidate for fabrication of tandem solar cells.

Sputtered ITO is widely used in semitransparent solar cells as the transparent electrode due to its high optical transparency in the visible and near-infrared (NIR) regions[82, 83]. Low resistivity and high optical transparency of sputtered ITO make it suitable as the tunnel recombination junction in tandem solar cells as well. In 2016, Snaith *et al*. firstly chose sputtering-deposited ITO as the charge recombination layer and ALD-deposited tin oxide (SnO_2) as the buffer layer, as shown in Fig. 4(e)[53]. The ITO layer was mainly used as the charge recombination layer and to protect the top subcell from being dissolved during subsequent perovskite processing. Here the SnO_2 layer was mainly deposited to protect the top subcell from sputtering. They obtained tandem solar cells with a PCE of 16.9% and a V_{oc} over 1.65 V. However, the J_{sc} values exhibited by the top and bottom subcells were not an ideal match (14.1 and 15.8 mA/cm^2).

Since then, ITO based tunnel recombination junction has been widely used in p–i–n structured all-perovskite tandem solar cells. The difference is that in order to reduce the damage to the top subcell during the sputtering process, different protective buffer layers are searched. Jen *et al*. sputtered ITO as the charge recombination layer on C_{60}/Bis-C_{60} (Fig. 4(f)). By combining a narrow-bandgap (1.2 eV) perovskite and a wide-bandgap (1.8 eV) perovskite, using indene-C_{60} bis-adduct ($IC_{60}BA$) as the electron transport layer, They achieved a V_{oc} of 1.98 V, which reached 80% of the theoretical limit[73]. Multi-layer structures as tunnel recombination junction are an effective way to improve device stability. Yan *et al*. designed a vacuum-processed multiple stack of ultrathin Ag (1 nm), MoO_x (3 nm) and ITO (~120 nm) as the tunnel recombination junction to construct a configuration of ITO/PTAA/$FA_{0.8}Cs_{0.2}Pb(I_{0.7}Br_{0.3})_3$/$C_{60}$/BCP/Ag/$MoO_x$/ITO/PEDOT:PSS/$(FASnI_3)_{0.6}(MAPbI_3)_{0.4}$/PCBM/BCP/Ag all-perovskite tandem solar cell[76]. A schematic of the tandem solar cell is shown in Fig. 4(g). Ag and MoO_x layers were deposited by thermal evaporation, and then ITO was sputtered on the MoO_x layer. The MoO_x layer prevented damaging to the BCP/Ag layers caused by the sputtering of ITO, and ensured good contact between Ag and ITO. The MoO_x layers make the top subcell film very smooth, forming a smooth, pinhole-free tunnel recombination junction that protects the top subcell from potential solvents during bottom subcell depositing processing, even the deposition of water-based PEDOT: PSS. In addition, the tunnel recombination junction had a transmittance of more than 70% in the range of 720 nm to nearly 900 nm, which ensured great light absorption of the bottom subcell. The champion device achieved a PCE of 20.6%. Moreover, better device performance cannot be achieved when the Ag layer or MoO_x layer is removed separately. Following that, Zhu *et al*. used the same structure to combine different components of perovskites, and achieved a PCE more than 23%[77]. They concluded that the PCE of tandem solar cells is mainly limited by the V_{oc} loss in the wide-bandgap perovskite and the low J_{sc} value in the device, and the optical loss of the tunnel recombination junction is the main reason for the low J_{sc}. The high-power deposition process and the large optical loss caused by the large refractive index of the ITO film are important factors that limit the further improvement of tandem device performance.

Atomic layer deposition (ALD) is the key technology for constructing a compact buffer layer. The use of a nucleation layer to improve the compactness of the tunnel recombination junction has recently been demonstrated by Moore *et al*.[63]. The schematic of the tandem solar cell is shown in Fig. 4(h). This strategy makes the ALD layer itself a barrier to effectively prevent sputtering and solvent damage.

During the same time, our group fabricated all-perovskite tandem solar cells with a configuration of glass/ITO/PTAA (poly(triarylamine)/wide-E_g perovskite/C_{60}/ALD-SnO_2/Au(~1 nm)/PEDOT:PSS/low-E_g perovskite/C_{60}/BCP/Cu[54]. The schematic about the tandem solar cell is shown in Fig. 4(i). This compact and robust ALD-SnO_2 layer (~20 nm) can efficiently prevent damage to the deposited-underlying top subcell during the solution processing of the bottom subcell, allowing the achievement of fabricating all-perovskite tandem solar cells without the ITO layer. The SnO_2 layer provides excellent electron extraction as well, resulting in a slight improvement in the performance of the wide-bandgap top subcell. An ultra-thin Au layer (~1 nm) was deposited on SnO_2 by thermal evaporation to promote electron-hole recombination. The champion tandem solar cell achieved the highest PCE of 24.8% reported so far, with a high V_{oc} of 1.965 V, a J_{sc} value of 15.6 mA/cm^2 and a high FF of 81%.

3.2. Progress in wide-bandgap perovskites

The performance of tandem solar cells closely depends on the performance of each. Compared with narrow-bandgap perovskites, wide-bandgap perovskites have been studies more extensively[84, 85]. In the previous works, wide-bandgap perovskites are used for tandem solar cells in combination with mature narrow-bandgap semiconductors, such as silicon[32–36], and chalcogenide[37–42].

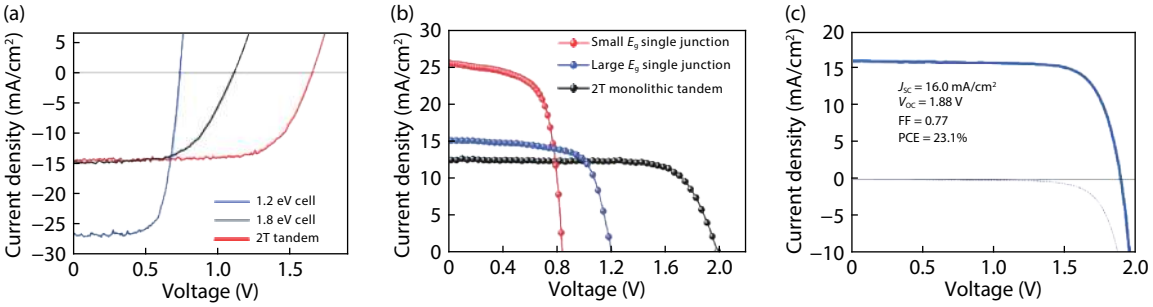

Fig. 5. (Color online) Performance of all-perovskite tandem solar cell with improved performance in the wide-bandgap top subcell. (a) *J*–*V* cures of tandem solar cell using $FA_{0.83}Cs_{0.17}Pb(I_{0.5}Br_{0.5})_3$ as the top subcell. Reproduced with permission[53]. (b) *J*–*V* cures of tandem solar cell using $MA_{0.9}Cs_{0.1}Pb(I_{0.6}Br_{0.4})$ as the top subcell. Reproduced with permission[73]. (c) *J*–*V* cures of tandem solar cell using $DMA_{0.1}FA_{0.6}Cs_{0.3}PbI_{2.4}Br_{0.6}$ as the top subcell. Reproduced with permission[63].

In the early stages of developing all-perovskite tandem solar cells, Im *et al.* and Ho-Baillie *et al.* used $CH_3NH_3PbBr_3$ (2.3 eV) as top subcell[52, 79]. The PCEs have been limited to ~10% due to the nonideal bandgap matching between subcells. In order to search a top subcell to match $MAPbI_3$ (1.55 eV) as the bottom subcell, Sessolo *et al.* synthesized a wide-bandgap perovskite of $Cs_{0.15}FA_{0.85}Pb(I_{0.3}Br_{0.7})_3$ (2 eV). The tandem solar cell achieved a PCE of 15.6%[72].

According to the bandgap matching rules in tandem solar cells, researchers often choose the combination of wide-bandgap (~1.8 eV) perovskites and narrow-bandgap (~1.2 eV) perovskites to fabricate tandem solar cells. In 2016, Snaith *et al.* achieved a high-efficiency, stable perovskite of $FA_{0.83}Cs_{0.17}Pb(I_{0.5}Br_{0.5})_3$ (1.8 eV) by using a mixture of FA^+ and Cs^+ cations and adjusting the Br^-/I^- ratio[53]. In a tandem solar cell using a perovskite layer with a 1.8 eV bandgap as the top subcell, they achieved a PCE of 16.9%, with a V_{oc} of 1.66 V, a J_{sc} value of 14.5 mA/cm^2 and a FF of 70%, as shown in Fig. 5(a).

In tandem solar cells, the V_{oc} is more provided by the wide-bandgap subcell[84]. The V_{oc} loss due to halide phase segregation is a common challenge for wide-bandgap perovskites. Introducing strain into the crystal lattice by ion doping, tilting of [BX_6] octahedron, introducing low-dimensional perovskite structures are strategies to widen the bandgap and to reduce the V_{oc} loss[85, 86]. Jen *et al.* alleviated the halide segregation in wide-bandgap perovskite by adding Cs^+ into $MAPb(I_{0.6}Br_{0.4})_3$ and obtained a more stable composition $MA_{0.9}Cs_{0.1}Pb(I_{0.6}Br_{0.4})$, as shown in Fig. 5(b)[73]. They obtained a subcell with a top transparent electrode by using a wide-bandgap (1.8 eV) perovskite, showing a V_{oc} of 1.22 V. In the all-perovskite tandem solar cell, a V_{oc} of 1.98 V was achieved, which reached 80% of the theoretical limit.

As a photostable perovskite component, $FA_{0.8}Cs_{0.2}Pb(I_{0.7}Br_{0.3})_3$ was also used as the top subcell in all-perovskite tandem solar cells[76]. Moore *et al.* fabricated single-junction PSCs using $DMA_{0.1}FA_{0.6}Cs_{0.3}PbI_{2.4}Br_{0.6}$, and achieved a PCE higher than 19% and a V_{oc} of 1.2 V, while the single-junction PSC without DMA only achieved a V_{oc} of 1.15 V. They fabricated tandem solar cells with a PCE of 23.1% by combining this wide-bandgap perovskite with a narrow-bandgap perovskite of $FA_{0.75}Cs_{0.25}Sn_{0.5}Pb_{0.5}I_3$, as shown in Fig. 5(c)[63].

3.3. Progress in narrow-bandgap perovskites

The PCE of all-perovskite tandem solar cells is still limited by the performance of mixed Pb–Sn narrow-bandgap PSCs. A thick absorber is required in mixed Pb–Sn PSCs to completely absorb the infrared light passing through the wide-bandgap cell[87]. The progress in mixed Pb–Sn narrow-bandgap perovskites paved the way for achieving highly efficient all-perovskite tandem solar cells. Snaith et al. firstly reported an all-perovskite tandem solar cell using $FA_{0.75}Cs_{0.25}Sn_{0.5}Pb_{0.5}I_3$ as the bottom subcell[53]. They used a strategy called precursor-phase anti-solvent immersion (PAI) to make a smooth, pinhole-free perovskite film, which took a low vapor pressure solvent to hinder crystallization and an anti-solvent bath to crystallize the film with only gentle heating[88, 89]. They achieved a stable, 14.8% efficient PSC based on a 1.2 eV bandgap $FA_{0.75}Cs_{0.25}Pb_{0.5}Sn_{0.5}I_3$ perovskite. Consequently, the PCE of the all-perovskite tandem solar cell they achieved was 16.9%, together with a V_{oc} of 1.66 V, and a J_{sc} value of 14.8 mA/cm^2.

Low V_{oc} is one of the main efficiency losses in narrow-bandgap PSCs. Considering the mismatch between the minimum conduction bands of $MAPb_{0.5}Sn_{0.5}I_3$ and C_{60}, Jen *et al.* used $IC_{60}BA$, an alternate fullerene derivative, as the electron transport layer to achieve better energy level alignment[73].

The fast crystallization of mixed Pb–Sn perovskites makes it difficult to achieve good film uniformity and good photoelectric performance, resulting in short carrier lifetimes of photogenerated s (typically one the order of ns)[53]. McGehee *et al.* reported a post-treatment using methylammonium chloride vapor to grow larger grains and to repair cracks in the deposited film, thereby increasing the V_{oc} and FF. After MACl post-processing and the addition of formic acid, the carrier lifetime was extended to nearly 0.5 μs, and the single-junction narrow-bandgap PSC achieved a stable PCE of 15.6%[75]. Tandem solar cells with a stabilized PCE of 19.1% was obtained. The top and bottom subcells showed J_{sc} values of 15.5 and 14.8 mA/cm^2, respectively. The EQE and *J*–*V* cures of this tandem solar cell are shown in Figs. 6(a) and 6(b).

Reducing non-radiative recombination loss in bulk perovskite is an important strategy to improve the performance of narrow-bandgap PSCs. Yan *et al.* introduced lead chloride in the precursor solution to expand the grain size, increases crystallinity and carrier mobility, and reduce the electronic disorder[76]. This enhancement allowed them to successfully process a high-efficiency, 700 nm-thick, 1.25 eV narrow-bandgap PSCs. The cells achieved a best PCE of 18.40% with a V_{oc} of 0.842 V, a J_{sc} value of 29.40 mA/cm^2 and a FF of 74.4%. With a 1.75 eV wide-bandgap perovskite top subcell,

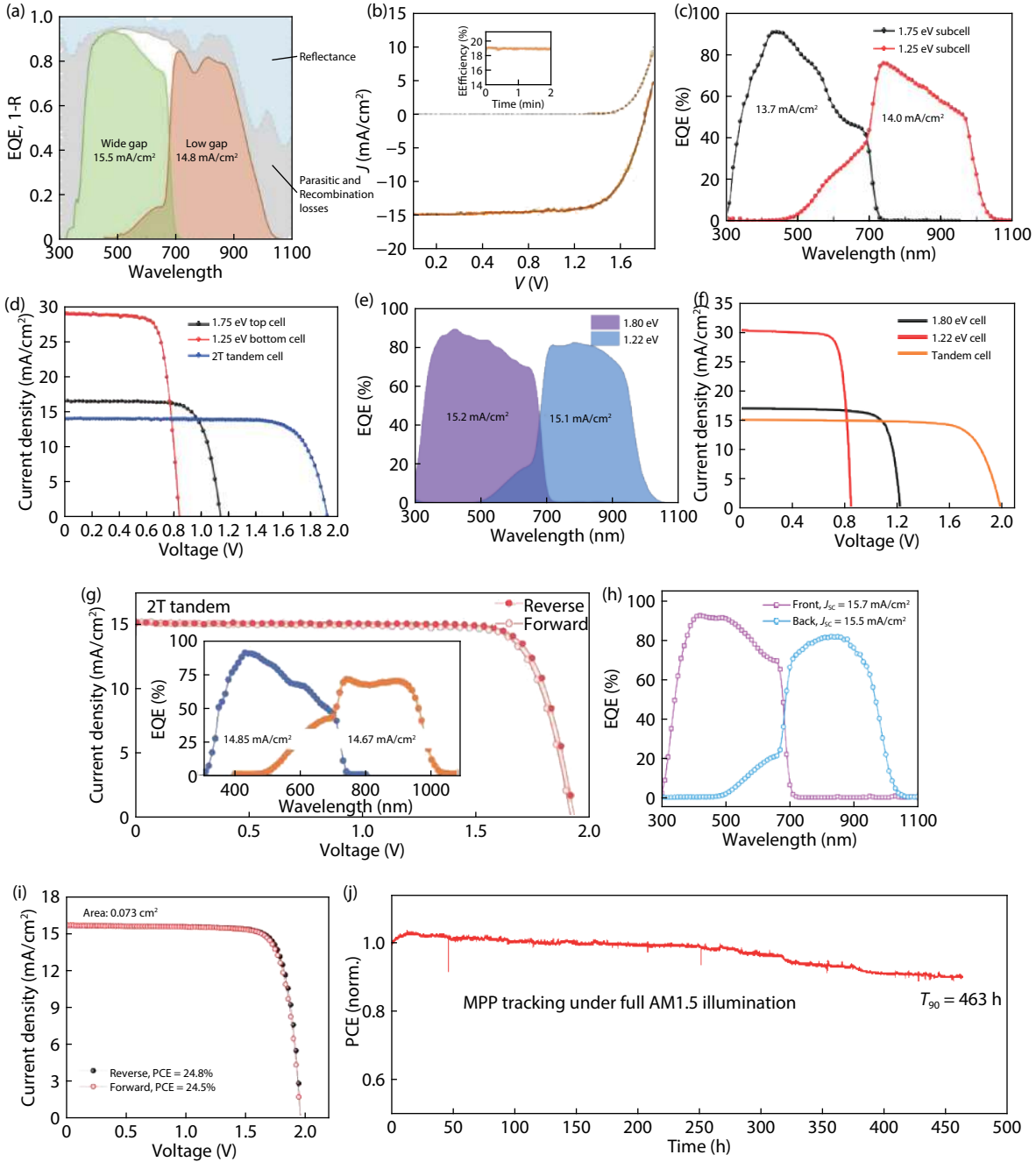

Fig. 6. (Color online) Performance of all-perovskite tandem solar cell with improved performance in the narrow-bandgap bottom subcell. (a, b) EQE and *J*–*V* cures of a tandem solar cell using $FA_{0.75}Cs_{0.25}Sn_{0.5}Pb_{0.5}I_3$ as the bottom subcell. Reproduced with permission[75]. (c, d) EQE and *J*–*V* cures of a tandem solar cell using $(FASnI_3)_{0.6}$ $(MAPbI_3)_{0.4}$-2.5%Cl as the bottom subcell. Reproduced with permission[76]. (e, f) EQE and *J*–*V* cures of a tandem solar cell using Cd-$FA_{0.5}MA_{0.45}Cs_{0.05}Pb_{0.5}Sn_{0.5}I_3$ as the bottom subcell. Reproduced with permission[90]. (g) EQE and *J*–*V* cures of a tandem solar cell using $(FASnI_3)_{0.6}(MAPbI_3)_{0.4}$ as the bottom subcell. Reproduced with permission[77]. (h–j) EQE and *J*–*V* cures and MPP of a tandem solar cell using $FA_{0.7}MA_{0.3}Pb_{0.5}Sn_{0.5}I_3$ as the bottom subcell. Reproduced with permission[54].

they achieved a PCE of 21% and a V_{oc} of 1.922 V in tandem solar cells. The EQE and *J*–*V* cures are shown in Fig. 6(c) and 6(d).

Huang *et al.* revealed that the charge collection efficiency in mixed Pb–Sn PSCs is mainly limited by a short diffusion length of electron[90]. They reduced the hole concentration and electron trap density by adding 0.03 mol% of Cd^{2+} into the precursor solution, and the electron diffusion length increased to 2.72 μm. They fabricated an all-perovskite tandem solar cell with a configuration of ITO/PTAA/$FA_{0.6}Cs_{0.4}Pb(I_{0.65}Br_{0.35})_3$/$C_{60}$/$SnO_2$/ITO/PEDOT:PSS/PTAA/Cd-$FA_{0.5}MA_{0.45}Cs_{0.05}Pb_{0.5}Sn_{0.5}I_3$/$C_{60}$/BCP/Cu, achieving a stable PCE of 22.7% in tandem cells. The EQE spectra showed that the J_{sc} values of the top and bottom subcells is 15.2 and 15.1 mA/cm^2, respectively, as shown in Figs. 6(e) and 6(f). Zhu *et al.* used guanidinium thiocyanate (GuaSCN) to improve the carrier diffusion length of narrow-bandgap mixed Pb–Sn perovskites to 2.5 μm[77]. Narrow-bandgap single-junction solar cells exhibited PCEs of 20.5% and 20.4% in forward and reverse scans, respectively. Following this strategy, the tandem solar cell achieved a PCE of 23.4%, with a V_{oc} of 1.942 V, a J_{sc} value of 15.01 mA/cm^2, and a FF of 80.31%. The EQE spectra showed

that the J_{sc} values of the top and bottom subcells are 14.85 and 14.67 mA/cm^2, respectively (Fig. 6(g)).

Recently, our group improved the carrier diffusion length up to 3 μm, and achieved a PCE of 21.1% in single-junction narrow-bandgap PSC with a bandgap of 1.22 eV[54]. We achieved this by reducing Sn vacancies caused by Sn^{2+} oxidation via a comproportionation reaction by adding Sn powders in the precursor solution. By increasing the thickness of the narrow-bandgap perovskite to 860 nm, we achieved maximum J_{sc} value above 32 mA/cm^2. The devices had high EQE values in the near infrared region. By combining a 1.77 eV wide-bandgap perovskite (about 300 nm), we fabricated all-perovskite tandem solar cells with a configuration of glass/ITO/PTAA/wide-E_g perovskite/C_{60}/ALD-SnO_2/Au (~1 nm)/PEDOT:PSS/low-E_g perovskite/C_{60}/BCP/Cu. We achieved a high PCE of 24.8%, with a V_{oc} of 1.965 V, a J_{sc} value of 15.6 mA/cm^2, and a high FF of 81% in a small-area tandem solar cell. The integrated J_{sc} values of the top and bottom subcells from EQE curves are 15.7 and 15.5 mA/cm^2, respectively. The EQE and *J*–*V* cures are shown in Figs. 6(h) and 6(i). The tandem solar cell retained 90% of initial performance following 463 h of operation at the maximum power point (MPP) under full 1-sun illumination (Fig. 6(j)). We also fabricated a large area all-perovskite tandem solar cell following the same process and achieved a high PEC of 22.3%.

4. Conclusion and perspective

The past five years have witnessed an impressively rapid progress in the development of all-perovskite tandem solar cells. The PCE has achieved a boost from less than 10% at the beginning to nearly 25% at present. However, there remain several challenges that need to be addressed to achieve higher PCEs beyond 30%. We suggest that researchers in the community shall pay close attention to following issues to obtain better performed all-perovskite tandem solar cells.

(1) Tunnel recombination junction is a crucial component in all-perovskite tandem solar cells. A tunnel recombination junction should have good optical transmission, low series resistance, sufficient robustness, large area processability, and low cost. Developing new tunnel recombination junctions is important to further reduce the parasitic absorption and V_{oc} loss.

(2) Large V_{oc} loss in wide-bandgap PSCs remains a considerable challenge for all-perovskite tandem solar cells. Phase segregation in wide-bandgap perovskite is one of the reasons for such large V_{oc} loss. In addition, interfacial recombination is another cause of V_{oc} loss.

(3) Achieving efficient tandem solar cell relies on high-performance mixed Pb–Sn PSCs. Oxidation of mixed Pb–Sn perovskites remains to be addressed for commercial viability.

In addition, current matching in tandem solar cells is one of the key factors that can affect the overall efficiency of the device. It is important to establish current matching by adjusting both the bandgaps and the thickness of perovskite subcells. Developing suitable encapsulation is another key factor ensure excellent environmental stability for commercial viability.

Acknowledegments

This work is financially supported by the National Key R&D Program of China (2018YFB1500102), National Natural Science Foundation of China (61974063), Natural Science Foundation of Jiangsu Province (BK20190315, BZ2018008), Program for Innovative Talents and Entrepreneur in Jiangsu, and Thousand Talent Program for Young Outstanding Scientists in China.

References

[1] Jung E H, Jeon N J, Park E Y, et al. Efficient, stable and scalable perovskite solar cells using poly (3-hexylthiophene). Nature, 2019, 567(7749), 511

[2] Luo D, Yang W, Wang Z, et al. Enhanced photovoltage for inverted planar heterojunction perovskite solar cells. Science, 2018, 360(6396), 1442

[3] Tan H, Jain A, Voznyy O, et al. Efficient and stable solution-processed planar perovskite solar cells via contact passivation. Science, 2017, 355(6326), 722

[4] Tsai H, Nie W, Blancon J C, et al. High-efficiency two-dimensional Ruddlesden–Popper perovskite solar cells. Nature, 2016, 536 (7616), 312

[5] Yang W S, Noh J H, Jeon N J, et al. High-performance photovoltaic perovskite layers fabricated through intramolecular exchange. Science, 2015, 348(6240), 1234

[6] Zhu P, Gu S, Luo X, et al. Simultaneous contact and grain-boundary passivation in planar perovskite solar cells using SnO_2-KCl composite electron transport layer. Adv Energy Mater, 2020, 10(3), 1903083

[7] Zhao Y, Tan H, Yuan H, et al. Perovskite seeding growth of formamidinium-lead-iodide-based perovskites for efficient and stable solar cells. Nat Commun, 2018, 9(1), 1607

[8] Han Q, Wei Y, Lin R, et al. Low-temperature processed inorganic hole transport layer for efficient and stable mixed Pb–Sn low-bandgap perovskite solar cells. Sci Bull, 2019, 64(19), 1399

[9] Kojima A, Teshima K, Shirai Y, et al. Organometal halide perovskites as visible-light sensitizers for photovoltaic cells. J Am Chem Soc, 2009, 131(17), 6050

[10] National Renewable Energy Laboratory. Best research-cell efficiencies. www.nrel.gov/ncpv/images/efficiency_chart.jpg, 2019

[11] Green M A, Dunlop E D, Levi D H, et al. Solar cell efficiency tables (version 54). Prog Photovolt Res Appl, 2019, 27(7), 565

[12] Shockley W, Queisser H J. Detailed balance limit of efficiency of p–n junction solar cells. J Appl Phys, 1961, 32(3), 510

[13] Geisz J F, Steiner M A, Jain N, et al. Building a six-junction inverted metamorphic concentrator solar cell. IEEE J Photovolt, 2017, 8(2), 626

[14] Meillaud F, Shah A, Droz C, et al. Efficiency limits for single-junction and tandem solar cells. Sol Energy Mater Sol Cells, 2006, 90(18/19), 2952

[15] Contreras M A, Mansfield L M, Egaas B, et al. Wide bandgap Cu(In, Ga)Se_2 solar cells with improved energy conversion efficiency. Prog Photovolt Res Appl, 2012, 20(7), 843

[16] Meng L, Zhang Y, Wan X, et al. Organic and solution-processed tandem solar cells with 17.3% efficiency. Science, 2018, 361(6407), 1094

[17] Che X, Li Y, Qu Y, et al. High fabrication yield organic tandem photovoltaics combining vacuum- and solution-processed subcells with 15% efficiency. Nat Energy, 2018, 3(5), 422

[18] Cheng P, Li G, Zhan X, et al. Next-generation organic photovoltaics based on non-fullerene acceptors. Nat Photonics, 2018, 12(3), 131

[19] Yuan J, Zhang Y, Zhou L, et al. Single-junction organic solar cell with over 15% efficiency using fused-ring acceptor with electron-deficient core. Joule, 2019, 3(4), 1140

[20] Anaya M, Lozano G, Calvo M E, et al. ABX_3 perovskites for tandem

solar cells. Joule, 2017, 1(4), 769
[21] Beal R E, Slotcavage D J, Leijtens T, et al. Cesium lead halide perovskites with improved stability for tandem solar cells. J Phys Chem Lett, 2016, 7(5), 746
[22] Yu Y, Wang C, Grice C R, et al. Synergistic effects of lead thiocyanate additive and solvent annealing on the performance of wide-bandgap perovskite solar cells. ACS Energy Lett, 2017, 2(5), 1177
[23] Leijtens T, Bush K A, Prasanna R, et al. Opportunities and challenges for tandem solar cells using metal halide perovskite semiconductors. Nat Energy, 2018, 3(10), 828
[24] Eperon G E, Stranks S D, Menelaou C, et al. Formamidinium lead trihalide: a broadly tunable perovskite for efficient planar heterojunction solar cells. Energy Environ Sci, 2014, 7(3), 982
[25] Xu G, Bi P, Wang S, et al. Integrating ultrathin bulk-heterojunction organic semiconductor intermediary for high-performance low-bandgap perovskite solar cells with low energy loss. Adv Funct Mater, 2018, 28(42), 1804427
[26] Wei M, Xiao K, Walters G, et al. Combining efficiency and stability in mixed tin–lead perovskite solar cells by capping grains with an ultrathin 2D layer. Adv Mater, 2020, 1907058
[27] Li C, Song Z, Zhao D, et al. Reducing saturation-current density to realize high-efficiency low-bandgap mixed tin–lead halide perovskite solar cells. Adv Energy Mater, 2019, 9(3), 1803135
[28] Liu X, Yang Z, Chueh C C, et al. Improved efficiency and stability of Pb–Sn binary perovskite solar cells by Cs substitution. J Mater Chem A, 2016, 4(46), 17939
[29] Yang Z, Rajagopal A, Chueh C C, et al. Stable low-bandgap Pb–Sn binary perovskites for tandem solar cells. Adv Mater, 2016, 28(40), 8990
[30] Zhao B, Abdi-Jalebi M, Tabachnyk M, et al. High open-circuit voltages in tin-rich low-bandgap perovskite-based planar heterojunction photovoltaics. Adv Mater, 2017, 29(2), 1604744
[31] Zhu H L, Choy W C H. Crystallization, properties, and challenges of low-bandgap Sn–Pb binary perovskites. Sol RRL, 2018, 2(10), 1800146
[32] Bush K A, Palmstrom A F, Zhengshan J Y, et al. 23.6%-efficient monolithic perovskite/silicon tandem solar cells with improved stability. Nat Energy, 2017, 2(4), 17009
[33] Werner J, Barraud L, Walter A, et al. Efficient near-infrared-transparent perovskite solar cells enabling direct comparison of 4-terminal and monolithic perovskite/silicon tandem cells. ACS Energy Lett, 2016, 1(2), 474
[34] Chen B, Zhengshan J Y, Manzoor S, et al. Blade-coated perovskites on textured silicon for 26%-efficient monolithic perovskite/silicon tandem solar cells. Joule, 2020, 4, 850
[35] Werner J, Weng C H, Walter A, et al. Efficient monolithic perovskite/silicon tandem solar cell with cell area > 1 cm^2. J Phys Chem Lett, 2016, 7(1), 161
[36] Duong T, Wu Y, Shen H, et al. Rubidium multication perovskite with optimized bandgap for perovskite-silicon tandem with over 26% efficiency. Adv Energy Mater, 2017, 7(14), 1700228
[37] Pisoni S, Fu F, Feurer T, et al. Flexible NIR-transparent perovskite solar cells for all-thin-film tandem photovoltaic devices. J Mater Chem A, 2017, 5(26), 13639
[38] Shen H, Peng J, Jacobs D, et al. Mechanically-stacked perovskite/CIGS tandem solar cells with efficiency of 23.9% and reduced oxygen sensitivity. Energy Environ Sci, 2018, 11(2), 394
[39] Todorov T, Gershon T, Gunawan O, et al. Perovskite-kesterite monolithic tandem solar cells with high open-circuit voltage. Appl Phys Lett, 2014, 105(17), 173902
[40] Han Q, Hsieh Y T, Meng L, et al. High-performance perovskite/Cu(In, Ga)Se_2 monolithic tandem solar cells. Science, 2018, 361(6405), 904
[41] Fu F, Feurer T, Weiss T P, et al. High-efficiency inverted semi-transparent planar perovskite solar cells in substrate configuration. Nat Energy, 2016, 2(1), 1690
[42] Bailie C D, Christoforo M G, Mailoa J P, et al. Semi-transparent perovskite solar cells for tandems with silicon and CIGS. Energy Environ Sci, 2015, 8(3), 956
[43] Zeng Q, Liu L, Xiao Z, et al. A two-terminal all-inorganic perovskite/organic tandem solar cell. Sci Bull, 2019, 64(13), 885
[44] Saha U, Alam M K. Proposition and computational analysis of a kesterite/kesterite tandem solar cell with enhanced efficiency. RSC Adv, 2017, 7(8), 4806
[45] Li Y, Hu H, Chen B, et al. Solution-processed perovskite-kesterite reflective tandem solar cells. Sol Energy, 2017, 155, 35
[46] Lee H, Lee C. Analysis of ion-diffusion-induced interface degradation in inverted perovskite solar cells via restoration of the Ag electrode. Adv Energy Mater, 2018, 8(11), 1702197
[47] Tanabe K. A Review of ultrahigh efficiency III–V semiconductor compound solar cells: multijunction tandem, lower dimensional, photonic up/down conversion and plasmonic nanometallic structures. Energies, 2009, 2(3), 504
[48] Ameri T, Li N, Brabec C J. Highly efficient organic tandem solar cells: a follow up review. Energy Environ Sci, 2013, 6(8), 2390
[49] Yu Z J, Leilaeioun M, Holman Z. Selecting tandem partners for silicon solar cells. Nat Energy, 2016, 1(11), 16137
[50] Celik I, Philips A B, Song Z, et al. Energy payback time (EPBT) and energy return on energy invested (eroi) of perovskite tandem photovoltaic solar cells. IEEE J Photovoltaics, 2017, 8(1), 305
[51] Zhengshan J Y, Carpenter J V, Holman Z C. Techno-economic viability of silicon-based tandem photovoltaic modules in the United States. Nat Energy, 2018, 3(9), 747
[52] Heo J H, Im S H. $CH_3NH_3PbBr_3$–$CH_3NH_3PbI_3$ perovskite–perovskite tandem solar cells with exceeding 2.2 V open circuit voltage. Adv Mater, 2016, 28(25), 5121
[53] Eperon G E, Leijtens T, Bush K A, et al. Perovskite-perovskite tandem photovoltaics with optimized band gaps. Science, 2016, 354(6314), 861
[54] Lin R, Xiao K, Qin Z, et al. Monolithic all-perovskite tandem solar cells with 24.8% efficiency exploiting comproportionation to suppress Sn (II) oxidation in precursor ink. Nat Energy, 2019, 4(10), 864
[55] Werner J, Niesen B, Ballif C. Perovskite/silicon tandem solar cells: Marriage of convenience or true love story? – An overview Adv Mater Interfaces, 2018, 5(1), 1700731
[56] Eperon G E, Hörantner M T, Snaith H J. Metal halide perovskite tandem and multiple-junction photovoltaics. Nat Rev Chem, 2017, 1(12), 0095
[57] Araújo G L, Martí A. Absolute limiting efficiencies for photovoltaic energy conversion. Sol Energy Mater Sol Cells, 1994, 33(2), 213
[58] Hörantner M T, Leijtens T, Ziffer M E, et al. The potential of multijunction perovskite solar cells. ACS Energy Lett, 2017, 2(10), 2506
[59] Unger E L, Kegelmann L, Suchan K, et al. Roadmap and roadblocks for the band gap tunability of metal halide perovskites. J Mater Chem A, 2017, 5(23), 11401
[60] Noh J H, Im S H, Heo J H, et al. Chemical management for colorful, efficient, and stable inorganic–organic hybrid nanostructured solar cells. Nano Lett, 2013, 13(4), 1764
[61] Chen W, Zhang J, Xu G, et al. A semitransparent inorganic perovskite film for overcoming ultraviolet light instability of organic solar cells and achieving 14.03% efficiency. Adv Mater, 2018, 30(21), 1800855
[62] Chen W, Chen H, Xu G, et al. Precise control of crystal growth for highly efficient $CsPbI_2Br$ perovskite solar cells. Joule, 2019, 3(1), 191
[63] Palmstrom A F, Eperon G E, Leijtens T, et al. Enabling flexible all-perovskite tandem solar cells. Joule, 2019, 3(9), 2193
[64] Saliba M, Matsui T, Domanski K, et al. Incorporation of rubidium cations into perovskite solar cells improves photovoltaic perform-

ance. Science, 2016, 354(6309), 206
[65] Park Y H, Jeong I, Bae S, et al. Inorganic rubidium cation as an enhancer for photovoltaic performance and moisture stability of $HC(NH_2)_2PbI_3$ perovskite solar cells. Adv Funct Mater, 2017, 27(16), 1605988
[66] Yadav P, Dar M I, Arora N, et al. The role of rubidium in multiple-cation-based high-efficiency perovskite solar cells. Adv Mater, 2017, 29(40), 1701077
[67] Zhang M, Yun J S, Ma Q, et al. High-efficiency rubidium-incorporated perovskite solar cells by gas quenching. ACS Energy Lett, 2017, 2(2), 438
[68] Liao W, Zhao D, Yu Y, et al. Fabrication of efficient low-bandgap perovskite solar cells by combining formamidinium tin iodide with methylammonium lead iodide. J Am Chem Soc, 2016, 138(38), 12360
[69] Im J, Stoumpos C C, Jin H, et al. Antagonism between spin-orbit coupling and steric effects causes anomalous band gap evolution in the perovskite photovoltaic materials $CH_3NH_3Sn_{1-x}Pb_xI_3$. J Phys Chem Lett, 2015, 6(17), 3503
[70] Prasanna R, Gold-Parker A, Leijtens T, et al. Band gap tuning via lattice contraction and octahedral tilting in perovskite materials for photovoltaics. J Am Chem Soc, 2017, 139(32), 11117
[71] Yang Z, Chueh C C, Liang P W, et al. Effects of formamidinium and bromide ion substitution in methylammonium lead triiodide toward high-performance perovskite solar cells. Nano Energy, 2016, 22, 328
[72] Forgács D, Gil-Escrig L, Pérez-Del-Rey D, et al. Efficient monolithic perovskite/perovskite tandem solar cells. Adv Energy Mater, 2017, 7(8), 1602121
[73] Rajagopal A, Yang Z, Jo S B, et al. Highly efficient perovskite–perovskite tandem solar cells reaching 80% of the theoretical limit in photovoltage. Adv Mater, 2017, 29(34), 1702140
[74] Jiang F, Liu T, Luo B, et al. A two-terminal perovskite/perovskite tandem solar cell. J Mater Chem A, 2016, 4(4), 1208
[75] Leijtens T, Prasanna R, Bush K A, et al. Tin–lead halide perovskites with improved thermal and air stability for efficient all-perovskite tandem solar cells. Sustain Energy Fuels, 2018, 2(11), 2450
[76] Zhao D, Chen C, Wang C, et al. Efficient two-terminal all-perovskite tandem solar cells enabled by high-quality low-bandgap absorber layers. Nat Energy, 2018, 3(12), 1093
[77] Tong J, Song Z, Kim D H, et al. Carrier lifetimes of $> 1\ \mu s$ in Sn–Pb perovskites enable efficient all-perovskite tandem solar cells. Science, 2019, 364(6439), 475
[78] Prasanna R, Leijtens T, Dunfield S P, et al. Design of low bandgap tin–lead halide perovskite solar cells to achieve thermal, atmospheric and operational stability. Nat Energy, 2019, 4(11), 939
[79] Sheng R, Hörantner M T, Wang Z, et al. Monolithic wide band gap perovskite/perovskite tandem solar cells with organic recombination layers. J Phys Chem C, 2017, 121(49), 27256
[80] Ávila J, Momblona C, Boix P, et al. High voltage vacuum-deposited $CH_3NH_3Pb_3$–$CH_3NH_3PbI_3$ tandem solar cells. Energy Environ Sci, 2018, 11(11), 3292
[81] Yan Y. All-perovskite tandem solar cell showing unprecedentedly high open-circuit voltage. Joule, 2018, 2(11), 2206
[82] Zhao D, Wang C, Song Z, et al. Four-terminal all-perovskite tandem solar cells achieving power conversion efficiencies exceeding 23%. ACS Energy Lett, 2018, 3(2), 305
[83] Abdollahi B, Hossain I M, Jakoby M, et al. Vacuum-assisted growth of low-bandgap thin films ($FA_{0.8}MA_{0.2}Sn_{0.5}Pb_{0.5}I_3$) for all-perovskite tandem solar cells. Adv Energy Mater, 2020, 10(5), 1902583
[84] Braly I L, Stoddard R J, Rajagopal A, et al. Current-induced phase segregation in mixed halide hybrid perovskites and its impact on two-terminal tandem solar cell design. ACS Energy Lett, 2017, 2(8), 1841
[85] Stoddard R J, Rajagopal A, Palmer R L, et al. Enhancing defect tolerance and phase stability of high-bandgap perovskites via guanidinium alloying. ACS Energy Lett, 2018, 3(6), 1261
[86] Saparov B, Mitzi D B. Organic–inorganic perovskites: structural versatility for functional materials design. Chem Rev, 2016, 116(7), 4558
[87] Zhao D, Yu Y, Wang C, et al. Low-bandgap mixed tin–lead iodide perovskite absorbers with long carrier lifetimes for all-perovskite tandem solar cells. Nat Energy, 2017, 2(4), 17018
[88] Hao F, Stoumpos C C, Guo P, et al. Solvent-mediated crystallization of $CH_3NH_3SnI_3$ films for heterojunction depleted perovskite solar cells. J Am Chem Soc, 2015, 137(35), 11445
[89] Zhou Y, Yang M, Wu W, et al. Room-temperature crystallization of hybrid-perovskite thin films via solvent–solvent extraction for high-performance solar cells. J Mater Chem A, 2015, 3(15), 8178
[90] Yang Z, Yu Z, Wei H, et al. Enhancing electron diffusion length in narrow-bandgap perovskites for efficient monolithic perovskite tandem solar cells. Nat Commun, 2019, 10(1), 4498